

## SODIUM-OXYGEN ANTICORRELATION AMONG HORIZONTAL BRANCH STARS IN THE GLOBULAR CLUSTER M4 \*

A. F. MARINO<sup>1</sup>, S. VILLANOVA<sup>2</sup>, A. P. MILONE<sup>3</sup>, G. PIOTTO<sup>3</sup>, K. LIND<sup>1</sup>, D. GEISLER<sup>2</sup>, AND P. B. STETSON<sup>4</sup>

*Draft version March 7, 2018*

### ABSTRACT

The horizontal branch (HB) morphology of globular clusters (GC) is mainly governed by metallicity. The second parameter problem, well known since the 60's, states that metallicity alone is not enough to describe the observed HB morphology of many GCs. Despite many efforts to resolve this issue, the second parameter phenomenon still remains without a satisfactory explanation. We have analyzed blue, red-HB, and RR-Lyrae stars in the GC M4 and studied their Fe, Na, and O abundances. Our goal is to investigate possible connections between the bimodal HB of M4 and the chemical signatures of the two stellar populations recently discovered among red giants of this cluster. We obtained FLAMES-UVES/GIRAFFE spectra of a sample of 22 stars covering the HB from the red to the blue region. While iron has the same abundance in both the red and blue-HB segment, the red-HB is composed of stars with scaled-solar sodium abundances, while the blue-HB stars are all sodium enhanced and oxygen depleted. The RR-Lyrae are Na-poor, as the red-HB stars, and O-rich. This is what we expect if the blue-HB consists of a second generation of stars formed from the ejecta produced by an earlier stellar population through high-temperature hydrogen-burning processes that include the CNO, NeNa, and MgAl cycles and are therefore expected to be He-rich. According to this scenario, the sodium and oxygen pattern detected in the blue and red-HB segments suggests helium as the second parameter that rules the HB morphology in M4.

*Subject headings:* globular clusters: individual (NGC 6121) — stars: abundances — stars: Population

### II

#### 1. INTRODUCTION

It is widely accepted that metallicity is the main parameter governing the horizontal branch (HB) morphology of globular clusters (GC), i.e. metal-rich GC stars preferentially populate the red side of the RR-Lyrae instability strip while metal-poor GCs tend to have blue HBs (e.g. Arp et al. 1952). However, since the 1960's several observations revealed that some GCs with similar metallicity exhibit different HB morphologies suggesting that a second parameter is needed to fully account for the HB extent (Sandage & Wallerstein 1960; Sandage & Wildey 1967).

Despite many efforts to understand the nature of the second parameter, it still remains one of the open issues of modern astrophysics. Several solutions have been proposed, including age, stellar mass, cluster central density, cluster mass (see Dotter et al. 2010 and references therein). Interestingly, a difference in helium could explain the observed HB morphology in GCs (van den Bergh 1967).

In this context, the recent discovery of multiple stellar populations in GCs (Piotto et al. 2007; Milone et al. 2008, 2010; Marino et al. 2009) allows us to look at the second parameter problem from a new point of view, as the

multiple HB components of several GCs have been tentatively assigned to different stellar generations by many authors (e.g. D'Antona et al. 2005, Milone et al. 2008).

The aim of this paper is to test whether stellar populations may be linked to the HB morphology in the nearby GC M4 (=NGC 6121). This cluster is an ideal target, as both spectroscopic and photometric studies have provided evidence that it experienced multiple star-formation events.

Chemical composition analysis of bright red giant branch (RGB) stars showed star-to-star variations in the C, N, O, Na, and Al abundances (Gratton et al. 1986, Brown et al. 1990, Brown & Wallerstein 1992, Drake et al. 1992), that define a clear CN distribution bimodality (Norris 1981), a Na-O anticorrelation, and a Na-Al correlation (Ivans et al. 1999; Marino et al. 2008, hereafter M08).

A bimodality in the distribution of stars on the Na-O anticorrelation in M4 has been found the recent analysis of high resolution spectra of 105 RGB stars by M08, who identified two stellar populations with a strong dichotomy in Na and O abundance. Na-rich stars are also CN-strong and are more Al-enriched than Na-poor ones. Neither any Mg-Al anticorrelation nor significant star-to-star variations in iron, iron-peak elements, *s*-process, or  $\alpha$  elements were detected.

The presence of two stellar populations in M4 is confirmed by photometry. The two groups of Na-rich/O-poor and Na-poor/O-rich stars define two distinct sequences in the  $U-(U-B)$  color-magnitude diagram (CMD). Na-rich stars populate a sequence on the red side of the RGB, while Na-poor ones define a bluer, broader sequence.

Interestingly, M4 has a bimodal HB, well populated

\*BASED ON DATA COLLECTED AT THE EUROPEAN SOUTHERN OBSERVATORY WITH THE VLT-UT2, PARANAL, CHILE.

<sup>1</sup> Max-Planck-Institut für Astrophysik, Postfach 1317, D-85741 Garching b. München, Germany; amarino@mpa-garching.mpg.de

<sup>2</sup> Departamento de Astronomía, Universidad de Concepción, Casilla 160-C, Concepción, Chile

<sup>3</sup> Department of Astronomy, University of Padova, Vicolo dell'osservatorio 3, 35122, Padova, Italy

<sup>4</sup> Herzberg Institute of Astrophysics, National Research Council Canada, 5071 West Saanich Road, Victoria, BC V9E 2E7

both on the blue and the red side of the RR-Lyrae gap. The existence of a physical connection between the CN-dichotomy observed on the RGB of this cluster and the HB morphology (the so-called second parameter problem) was already suggested by Norris (1981). The first evidence of such a connection came from Smith & Norris (1993), who found that the majority of the red-HB stars in M4 have a similar strong CN content. Nevertheless, from the Smith & Norris (1993) study one could tentatively associate the red-HB with the N-rich/C-poor/N-rich stars, the analysis of one blue-HB star done by Lambert et al. (1992), reveals that it could be the counterpart of a C-poor RGB star. We note, however, that Smith & Norris (1993) expressed caution concerning their absolute measures of the CN abundances, but stated that the CN abundance was similar in the analyzed red-HB stars.

In this paper we investigate the possibility that the HB bimodality in M4 could be related with the two stellar populations identified by M08 by investigating chemical abundances directly on HB stars.

## 2. OBSERVATIONS AND DATA ANALYSIS

The data set consists of high and medium resolution spectra obtained with the FLAMES/UVES (set-up 520nm,  $R \sim 47,000$ ) and FLAMES/GIRAFFE (set-ups HR11, HR13, HR15N,  $R \sim 20,000$ ) spectrographs (runs: 71.D-0205A, 083.B-0083A). These data were reduced using the dedicated pipelines (<http://girblid-rs.sourceforge.net> for GIRAFFE and Ballester et al. 2000 for UVES). On the basis of the position on the CMD, represented in Fig.1 (see Sect 2.1 for more details), our sample includes 6 blue-HB (blue symbols) and 16 stars distributed on the red side (red symbols). Two of the latter have been observed with UVES (red circles) and 14 with GIRAFFE (red crosses). For 16 red stars we derived Fe and Na, and, for the UVES targets only, O abundances.

Each star observed with UVES has from 2 to 4 exposures, and the final combined spectra have a typical S/N ranging from  $\sim 60$  in the bluer part of the spectrum, to  $\sim 90$  in the redder one ( $\lambda \sim 6150 \text{ \AA}$ ), where the O triplet that we measured is located. GIRAFFE spectra for each star were obtained by co-adding 10 exposures, and have a higher S/N, ranging from  $\sim 150$  for the HR11 set-up to  $\sim 250$  for the HR15N one.

We have identified all but one (GIRAFFE #47328), stars in the catalog of Cudworth & Rees (1990), and found that the two stars observed with UVES on the red part of the HB are RR-Lyrae variables listed in the catalog by Sawyer-Hogg (1973).

Chemical abundances for iron were derived from equivalent widths (EW), by using the local thermodynamical equilibrium (LTE) code MOOG (Snedden 1973), coupled with model atmospheres interpolated from the grid of ATLAS9 models (Castelli & Kurucz 2004). The linelist was extracted by M08, and the atomic linelist by Qiu et al. (2001), more appropriate for warmer stars. We used Fe lines to derive the atmospheric parameters ( $T_{\text{eff}}$ ,  $\log g$ ,  $\xi_t$ , and  $[\text{Fe}/\text{H}]^5$ ):  $T_{\text{eff}}$  and  $\xi_t$  were derived by removing trends in Fe I abundances with excitation potential and with EWs respectively; gravities  $\log g$  by satisfying

the ionization equilibrium between Fe I and Fe II abundances. This process was done iteratively until a final interpolated model was obtained.

Sodium was measured from EWs of the doublets at  $\sim 5890 \text{ \AA}$  and  $\sim 5685 \text{ \AA}$ . For the blue-HB stars, that have  $T_{\text{eff}} \gtrsim 8000$ , we were not able to measure the weak doublet at  $\sim 5685 \text{ \AA}$ , while for the two RR-Lyrae observed with UVES, we derived Na from the weak doublet, discarding the very strong lines at  $\sim 5890 \text{ \AA}$ , since at these temperatures, they get too strong for accurate abundance measurements. For stars observed with GIRAFFE, due to the lower resolution, we used a spectral synthesis analysis of the weak doublet at  $\sim 5685 \text{ \AA}$ . As Na spectral lines for our stars are heavily affected by departures from LTE that depends also on the spectral line strengths, we derive sodium in the non-LTE regime, by generating non-LTE profiles using the non-LTE spectral code MULTI (Carlsson 1986; see Lind et al. *subm.* for a description of the non-LTE modeling) coupled with our Kurucz model atmospheres. As an example, we show in the upper panel of Fig. 3 the observed Na lines for the blue-HB star #22746 with superimposed the non-LTE profiles. We quoted the Na abundances obtained for this star in the non-LTE regime.

Oxygen was estimated from spectral synthesis to the triplet at  $\sim 6157 \text{ \AA}$  available for UVES. Synthetic spectra at different O were matched with the observed spectrum, and we choose the best fit model by minimizing the  $\chi^2$  with respect to the observed spectrum. For O, expected non-LTE effects ( $\lesssim 0.1$  dex) are less significant than for Na, hence we applied corrections available in the literature (Takeda et al. 1997).

Non-LTE effects could also affect the Fe lines. However, in our analysis, we did not consider non-LTE corrections for Fe lines, that should not affect significantly the ionization equilibrium (Villanova et al. 2009).

To investigate the reliability of our atmospheric parameters we did the tests represented in Fig. 2. In the left panel, we compared our adopted  $T_{\text{eff}}$  with those derived by isochrones by D'Antona et al. (2009), coupled with our photometric data. Our sample of stars distributes with a dispersion of  $\sim 50 \text{ K}$  around the line of perfect agreement. The dispersion is similar for the red-HB stars observed with GIRAFFE and the blue-HB stars observed with UVES. This value has been taken as a rough estimate of the error associated to our temperatures, of course this is only internal. As expected since the photometric data have not been taken contemporary to the spectra, the two RR-Lyrae show a larger scatter from the line of perfect agreement. To verify whether our  $T_{\text{eff}}$  scale is correct, we compared the observed  $(B - V)$  colors with the synthetic Kurucz's colors  $(B - V)_{\text{Castelli}}$  (Castelli 1999). For this purpose we dereddened our colors by assuming  $E(B - V) = 0.36$  (Harris 1996). These tests are shown in the two right panels of Fig.2, where the observed  $(B - V)$  and the adopted  $T_{\text{eff}}$  for the blue-HB stars (upper panel), and red-HB plus RR-Lyrae stars (lower panel) have been compared with the  $(B - V)_{\text{Castelli}}$  at  $[\text{A}/\text{H}] = -1$ , for different gravities. Figure 2 suggests that the internal uncertainty associated to our  $\log g$  measurements is 0.25. Red-HB stars distribute in agreement with what expected from synthetic colors. Their position on the  $T_{\text{eff}} - (B - V)_{\text{Castelli}}$  plane are much less sensitive to

<sup>5</sup> We use  $[\text{Fe}/\text{H}]$  synonymously with stellar overall metallicity.

gravity (as an example we plotted the tracks corresponding to  $\log g=2.5$  and  $\log g=4.0$ ). However, since these stars have almost the same magnitude, we expect them to have a similar gravity. Hence, the rms of the  $\log g$  values obtained for these stars, that is 0.17, could be taken as an estimate for the internal uncertainty related to gravities. The error in  $\xi_t$  has been estimated following the procedure described in M08: i) we calculated for each star the error associated with the slope of the best least squares fit in the relation between Fe I abundances vs. reduced EWs; ii) we varied microturbulence until the slope of the best fitting line in the Fe I-EWs relation is equal to this error; iii) the corresponding difference in the  $\xi_t$ , ( $\sim 0.20$  km/s), has been taken as an estimate of the internal uncertainty associated with this parameter.

The limited S/N of the spectra imply an error in the placement of the continuum both for the EW measurements and the spectral synthesis. The mean difference in EWs among the same lines observed in pairs of stars with similar atmospheric parameters, that is  $\langle \Delta \text{EW} \rangle \simeq 5$  mÅ for UVES, and slightly lower for GIRAFFE, thanks to the high S/N, is an estimate of these uncertainties. To verify how model atmosphere and EW uncertainties influence the derived chemical abundances, we repeated the abundance measurements for one RR-Lyrae star (#34211), one blue-HB star (#27613), and one red-HB star (#46113). For this exercise, one by one at a time, we changed the uncertain parameters by  $\Delta T_{\text{eff}} = \pm 50$  K,  $\Delta \log g = \pm 0.25$ ,  $\Delta \xi_t = \pm 0.20$ ,  $\Delta [A/H] = \pm 0.2$ ,  $\Delta \text{EW} = 5$  mÅ respectively. Assuming that these uncertainties are uncorrelated, we estimate total abundance uncertainties by summing in quadrature the various contributions. The resulting internal errors are typically of  $\sim 0.10$  dex for the iron abundances, and  $\sim 0.05$  dex for the Na abundance ratios relative to iron. We also test the  $[\text{Na}/\text{Fe}]$  sensitivities to changes in temperature of  $\pm 100$  K, and verified that the Na abundance ratios are affected at a level of  $\lesssim 0.10$ . Oxygen abundance ratios are marginally affected by model uncertainties: while its abundance ratio is almost insensible to changes in  $T_{\text{eff}}$ , changes in  $\log g$  of  $\pm 0.2$  affect the  $[\text{O}/\text{Fe}]$  abundances of  $\mp 0.02$ . However, in this case, the dominant error source is the continuum placement, that strongly depends on the S/N of our spectra, and allows us to define the best fit among the observed and synthetic spectra with an uncertainty of  $\sim 0.10$  dex. An example of the O synthesis has been shown in the lower panel of Fig. 3, where we show the best fit synthesis, and deviations of  $\pm 0.2$  from the best fit.

The linelist with derived EWs, is listed in the on-line available Table 2. The photometry, adopted atmospheric parameters, chemical contents, and applied non-LTE corrections, are listed in Table 1.

### 2.1. Photometry

Our photometry provided by Stetson, has been already described in D'Antona et al. (2009). The observed colors and magnitudes have been corrected for differential reddening, and proper motions (Anderson et al. 2006) are used to separate field from cluster stars.

In the  $V-(B-I)$  CMD corrected for differential reddening of Fig. 1 we plotted only stars assumed to be cluster members, separated from the field as shown in the right-hand panels, with the proper motion vector point dia-

grams for four magnitude intervals. In these panels DX and DY are the proper motions in pixels. Proper motions are calculated with respect to a sample of cluster stars, and therefore member stars define a narrow bulk of stars centered around  $DX=DY=0$ . Red circles isolate the objects that have member-like motions (black dots). To correct for differential reddening, we used the method described in Milone et al. (2010, 2010 in prep). Briefly, we define the fiducial main sequence and estimate for each star, how the stars in its vicinity may systematically lie to the red or the blue of the fiducial sequence; this systematic color offset is indicative of the local differential reddening.

### 3. RESULTS

In this section we present the obtained abundances, and compare chemical properties of the blue, red-HB and RR-Lyrae stars.

Our analysis confirms that M4 has an average iron abundance of:

$$[\text{Fe}/\text{H}] = -1.12 \pm 0.02$$

(internal error) in agreement, within errors, with results obtained on RGB stars by M08. This in turn confirms that our study is not affected by significant systematic errors. There is no significant difference in the average  $[\text{Fe}/\text{H}]$  of stars located on different HB segments, as the mean iron abundances derived for blue-HB stars agrees, within the errors, with the one obtained for red-HB and RR-Lyrae ( $[\text{Fe}/\text{H}]_{\text{blue-HB}} = -1.07 \pm 0.02$  and  $[\text{Fe}/\text{H}]_{\text{red-HB+RR-Lyrae}} = -1.14 \pm 0.03$ ).

On the contrary, we detected large star-to-star variations in  $[\text{Na}/\text{Fe}]$ . All the red-HB stars have lower sodium, with  $[\text{Na}/\text{Fe}]$  ranging from  $\sim -0.2$  to  $\sim +0.2$  dex, average:

$$[\text{Na}/\text{Fe}]_{\text{red-HB+RR-Lyrae}} = -0.01 \pm 0.01$$

(internal error), and observed dispersion of  $\sim 0.10$  dex.

Conversely, the blue-HB stars all have high sodium, between  $\sim +0.25$  and  $\sim +0.40$ , with average:

$$[\text{Na}/\text{Fe}]_{\text{blue-HB}} = +0.34 \pm 0.02$$

(internal error) and an observed dispersion of  $\sim 0.06$  dex.

The two RR-Lyrae have a mean  $[\text{Na}/\text{Fe}]_{\text{RR-Lyrae}} = 0.04$ , in concert with the red-HB stars.

For one blue-HB star (#36648), we were able to measure Na from one line of the weak doublet, that gives enhanced Na abundance as obtained from the resonance doublet. This comparison allow to safely discard systematics introduced by the analysis of different spectral lines as the cause of the observed differences in Na.

In Fig. 4 we highlight the relation between the position of stars along the HB ( $B-I$ ) and their sodium abundances: a clear anticorrelation between the observed ( $B-I$ ) and the sodium abundance is present, with blue and red-HB+RR-Lyrae stars clustered around two distinct values of color and  $[\text{Na}/\text{Fe}]$ .

Oxygen has been measured for the stars observed with UVES, i.e. the whole sample of blue-HB stars and the two RR-Lyrae. The blue-HB stars have an average oxygen of:

$$[\text{O}/\text{Fe}]_{\text{blue-HB}} = +0.27 \pm 0.02$$

(internal error only) and an observed dispersion of  $\sim 0.05$  dex. The two variables for which we were able to see the O lines have higher O content. For GIRAFFE targets we could not estimate the O content because the forbidden line is too weak. The RR-Lyrae turn out to be enriched in O with a mean of  $[\text{O}/\text{Fe}]_{\text{red-HB}} = +0.50 \pm 0.01$ .

The present O and Na results are in good agreement with those found from high resolution UVES spectra of 105 RGB stars by M08. In Fig. 4 we show the Na-O anticorrelation for the RGB stars (gray squares) from M08, and the HB stars analyzed here. We arbitrarily plotted the RHB stars observed with GIRAFFE, for which oxygen abundances are not available, at  $[\text{O}/\text{Fe}] = +0.70$ . As already discussed in Sect. 1, from their study of RGB stars M08 detected two stellar populations in M4 with different sodium, oxygen, and CN abundances. The two groups of Na-poor/O-rich and Na-rich/O-poor stars define the Na-O anticorrelation of Fig. 4, and trace two branches on the RGB when the  $(U - B)$  color is used.

Apart from possible small zero-point displacements, likely due to the use of different spectral lines and non-LTE corrections, the HB stars analyzed here follow the trend defined by the giants. The blue-HB stars lie in the O-poor/Na-rich group, while the red-HB ones belong to the O-rich/Na-poor stellar population. Possible enhancements in He do not affect the  $[\text{X}/\text{Fe}]$  abundance measurements of these gravity-insensitive species (Lind et al. subm.).

Interestingly, the two RR-Lyrae belong to the Na-poor/O-rich population, corresponding to the first stellar generation.

#### 4. CONCLUSIONS

In this paper we studied a sample of HB stars in the GC M4, with the main purpose of measuring their abundance of sodium and oxygen. Our targets exhibit a bimodal Na distribution very similar to that found for RGB stars, with red-HB stars having roughly solar-scaled  $[\text{Na}/\text{Fe}]$  and blue-HB stars being all sodium enhanced. Blue-HB stars are also oxygen depleted, while the two variables are oxygen rich, and sodium poor as well as the red-HB stars.

The Na-O anticorrelation of HB stars is almost the same as we found for RGB stars, where we detected

two distinct stellar populations with different mean Na and O. *On the basis of their position in the Na-O plane, the blue-HB stars can be clearly associated with the second (O-poor/Na-rich) stellar generation, while the red-HB and the RR-Lyrae must be the progeny of the O-rich/Na-poor first generation.*

As already mentioned in Sect. 1, the Na-O anticorrelation is a powerful tracer of the star formation history in a GC. It has been observed among unevolved stars in GCs (Gratton et al. 2001), demonstrating that this pattern is not the result of some mixing process but is rather produced by the ejecta of a first stellar generation. It is not a property of a few peculiar objects but has been observed in all the GCs studied so far. While it is now widely accepted that it indicates the presence of material gone through high temperature H-burning processes, which include the CNO, NeNa, and MgAl cycles, the nature of the polluters is still unclear. These processes might have occurred in intermediate-mass asymptotic giant branch stars (D'Antona et al. 2002) or in fast-rotating massive stars (Decressin et al. 2007). In any case, helium is the main product of H-burning and is expected to be related to Na and O abundance, with stars that are Na-enhanced and O-depleted being also He-enriched.

According to this scenario, the present day He-rich (Na-rich, O-poor) stars should be less massive than He-poor (Na-poor, O rich) ones because the latter evolve more slowly. As a consequence of this, the blue-HB should consist of He/Na-rich, O-poor stars, while the He/Na-poor, O-rich stellar population should end up on the red-HB (D'Antona et al. 2002). The abundances of sodium and oxygen in HB stars presented in this paper strongly support this picture.

Our results show that in M4 the spread of light elements is strongly correlated with the HB morphology. It is tempting to affirm that, at least in this cluster, this spread is the *second parameter*, with He possibly being the main driver of its HB morphology after Fe.

*Acknowledgements* We thank the referee whose suggestions have improved significantly the paper, M. Bergemann, L. Mashonkina, F. D'Antona for useful discussions. AFM, APM, and GP acknowledge the support by MIUR under the PRIN2007 (prot.20075TP5K9).

#### REFERENCES

- Alcaino, G. 1975, *A&AS*, 21, 5  
 Anderson, J., Bedin, L.R., Piotto, G., Yadav, R.S., & Bellini, A. 2006, *A&A*, 454, 1029  
 Arp, H.C., Baum, W.A., & Sandage, A.R. 1952, *AJ*, 57, 4  
 Ballester, P., Modigliani, A., Boitquin, O., Cristiani, S., Hanuschik, R., Kaufer, A., & Wolf, S. 2000, *The Messenger*, 101, 31  
 Brown, J.A., Wallerstein, G., & Oke, J.B. 1990, *AJ*, 100, 1561  
 Brown, J.A., & Wallerstein, G. 1992, *AJ*, 104, 1818  
 Carlsson, M. 1986, *Uppsala Astronomical Observatory Reports*, 33  
 Castelli, F. 1999, *A&A*, 346, 564  
 Castelli, F., & Kurucz, R. L. 2004, arXiv:astro-ph/0405087  
 Cudworth, K. M., & Rees, R. 1990, *AJ*, 99, 1491  
 D'Antona, F., Caloi, V., Montalbán, J., Ventura, P., & Gratton, R. 2002, *A&A*, 395, 69  
 D'Antona, F., Bellazzini, M., Caloi, V., Fusi Pecci, F., Galletti, S., & Rood, R. T., 2005, *ApJ*, 631, 868  
 D'Antona, F., Stetson, P.B., Ventura, P., Milone, A.P., Piotto, G., & Caloi, V. 2009, *MNRAS*, 399, 151  
 Decressin, T., Meynet, G., Charbonnel, C., Prantzos, N. & Ekström, S., 2007, *A&A*, 464, 1029  
 Dotter, A., Sarajedini, A., Anderson, J., Aparicio, A., Bedin, L.R., Chaboyer, B., Majewski, S., Marín-Franch, A., Milone, A., et al. 2010, *ApJ*, 708, 698  
 Drake, J.J., Smith, V.V., & Suntzeff, N.B. 1992, *ApJ*, 395, 95  
 Gratton, R.G., Quarta, M.L., & Ortolani, S. 1986, *A&A*, 169, 208  
 Gratton, R.G., Bonifacio, P., Bragaglia, A., Carretta, E., Castellani, V., Centurion, M., Chieffi, A., Claudi, R., et al. 2001, *A&A*, 369, 87  
 Harris, W. E. 1996, *VizieR Online Data Catalog*, 7195, 0  
 Ivans, I.I., Sneden, C. Kraft, R.P., Suntzeff, N.B., Smith, V.V., Langer, G.E., & Fulbright, J.P. 1999, *AJ*, 118, 1273  
 Lambert, D. L., McWilliam, A., & Smith, V. V. 1992, *ApJ*, 386, 685  
 Lee, S.-W. 1977, *A&AS*, 27, 367  
 Lind K., Asplund M., Barklem P.S. & Belyaev A.K., submitted to *A&A*  
 Lind K., Charbonell C., Decressin T. & Primas F., Grundahl F., Asplund M. submitted to *A&A*  
 Marino, A. F., Villanova, S., Piotto, G., Milone, A. P., Momany, Y., Bedin, L. R., & Medling, A. M. 2008, *A&A*, 490, 625

Marino, A. F., Milone, A. P., Piotto, G., Villanova, S., Bedin, L. R.,  
 Bellini, A., & Renzini, A. 2009, *A&A*, 505, 1099  
 Milone, A. P. et al. 2008, *ApJ*, 673, 241  
 Milone, A. P., et al. 2010, *ApJ*, 709, 1183  
 Milone et al. in preparation  
 Norris, J. 1981, *ApJ*, 248, 177  
 Piotto, G. et al. 2007, *ApJ*, 661, L53  
 Qiu, H.M., Zhao, G., Chen, Y.Q., & Li, Z.W. 2001, *ApJ*, 548, 953  
 Sandage, A., & Wallerstein, G. 1960, *ApJ*, 131, 598

Sandage, A., & Wildey, R. 1967, *ApJ*, 150, 469  
 Sawyer Hogg, H. 1973, *Publications of the David Dunlap  
 Observatory*, 3, 6  
 Smith, G. H., & Norris, J. E. 1993, *AJ*, 105, 173  
 Sneden, C. A. 1973, Ph.D. Thesis  
 Takeda, Y. 1997, *PASJ*, 49, 471  
 van den Bergh, S. 1967, *AJ*, 72, 70

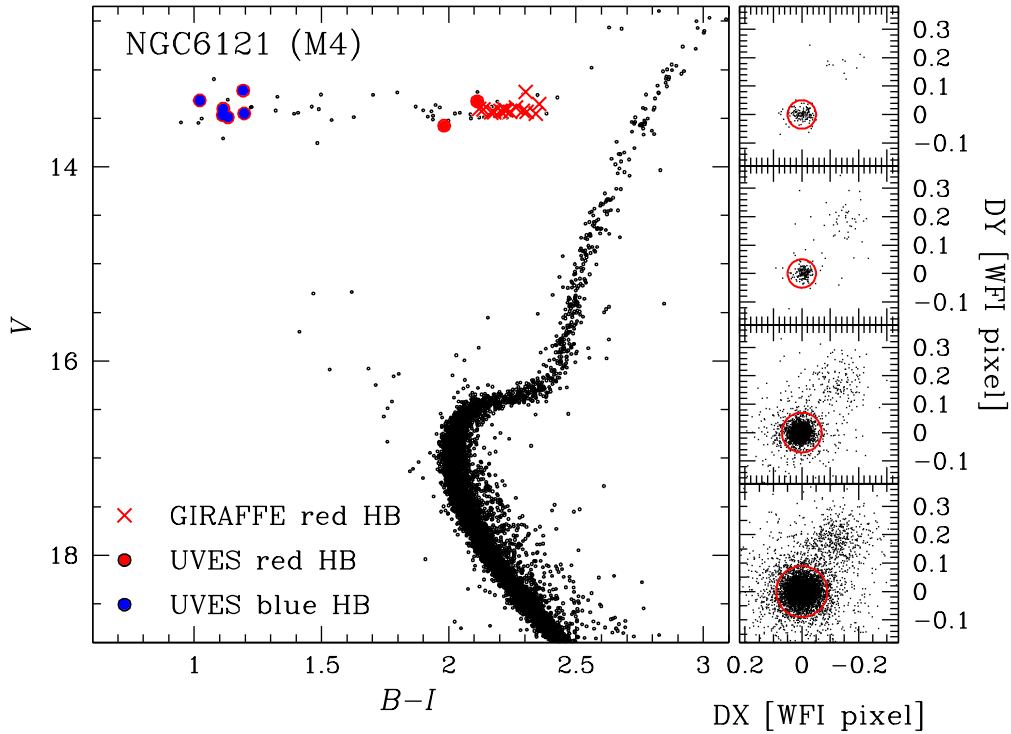


FIG. 1.— CMD corrected for differential reddening for all stars assumed to be cluster members. UVES and GIRAFFE targets are marked with circles and crosses respectively. Blue and red colors represent stars in the blue and red-HB, respectively. On the right panels we represent proper motion diagrams for stars in the M4 field of view in four magnitude intervals. A circle shows the adopted membership criterion.

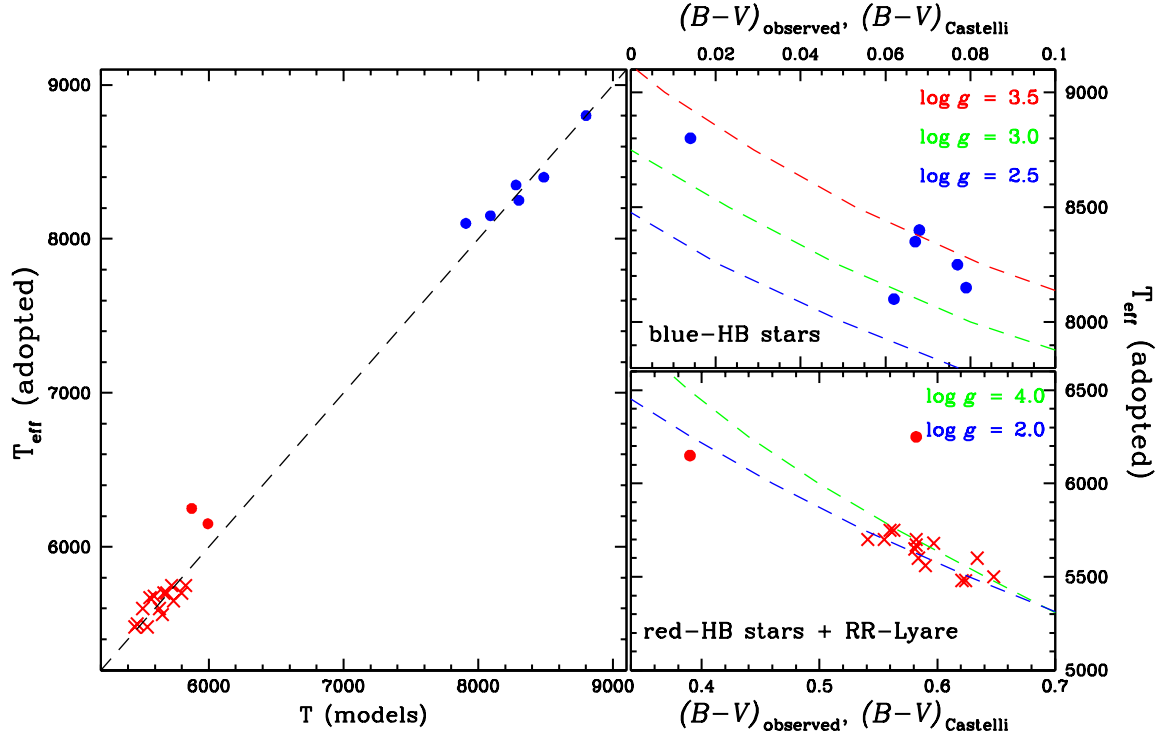


FIG. 2.— *Left* : Adopted  $T_{\text{eff}}$  vs. of the temperature derived from isochrones and observed colors. Dashed line represents the perfect agreement. *Right* : Adopted  $T_{\text{eff}}$  versus observed  $((B - V)_{\text{observed}})$  for the blue-HB stars (upper panel) and the red-HB+RR-Lyrae stars (lower panel). Dashed lines represent tracks obtained from the synthetic colors  $((B - V)_{\text{Castelli}})$  at different gravities. The  $\log g$  corresponding to each track has been quoted in both panels.

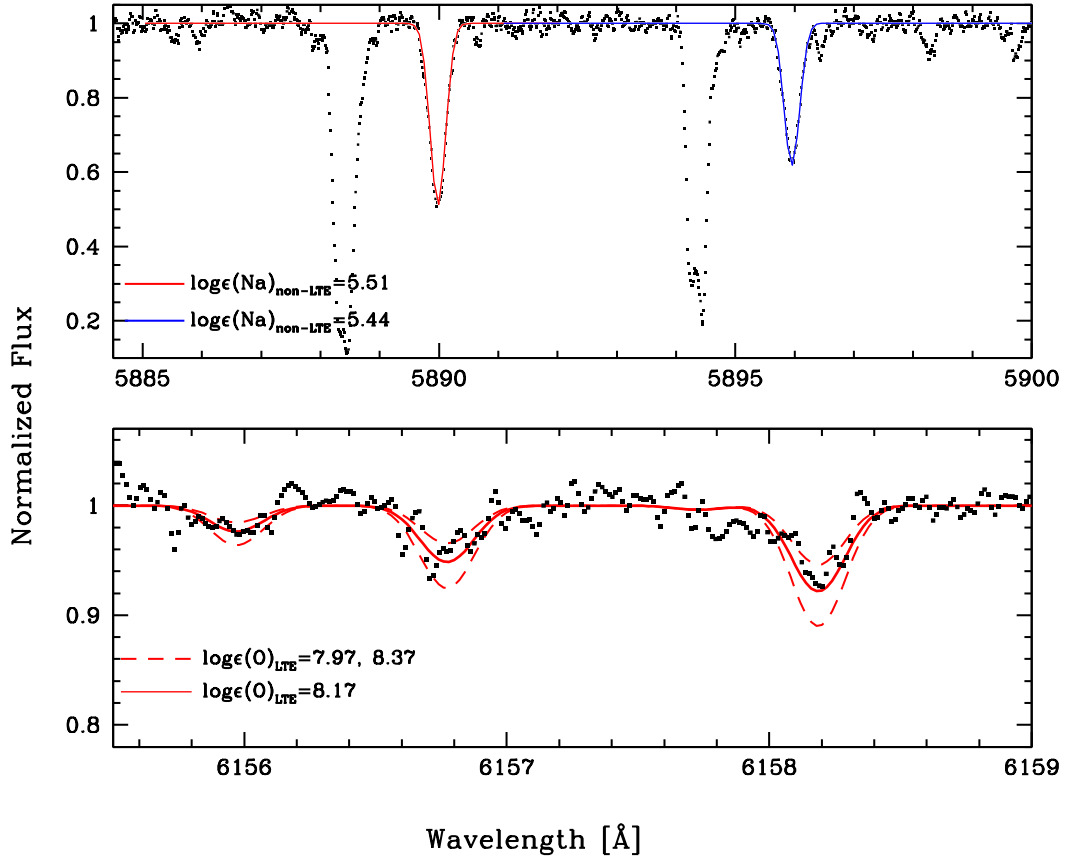


FIG. 3.— *Upper Panel:* non-LTE profiles for the two Na lines of the star #22746. The abundances obtained by each line is quoted in the panel. *Lower panel:* Example of O spectral line fitting for the star #36648. Synthetic spectra with differences in abundance of  $-0.20$ ,  $+0.00$ ,  $+0.20$  dex with respect to the adopted value are shown.

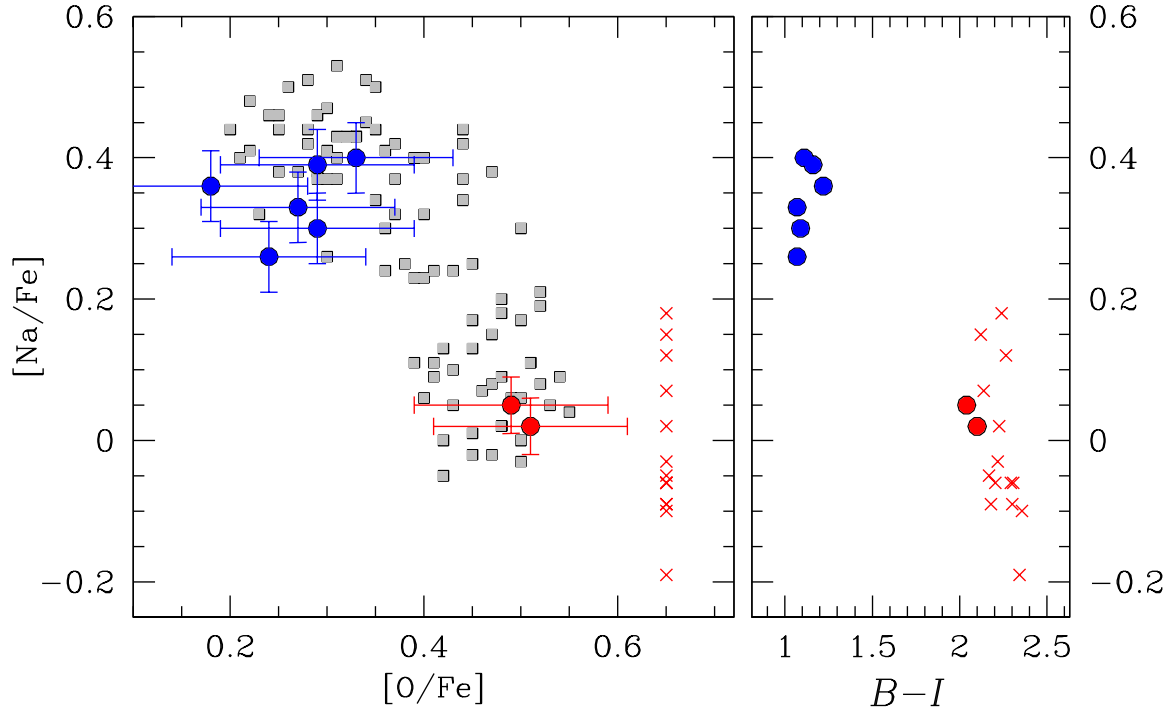


FIG. 4.— *Left:*  $[\text{Na}/\text{Fe}]$  versus  $[\text{O}/\text{Fe}]$  for UVES stars represented with blue and red circles. Red crosses indicate the GIRAFFE red-HB stars for which  $[\text{O}/\text{Fe}]$  is not available. As a comparison, we show as gray squares  $[\text{Na}/\text{Fe}]$  and  $[\text{O}/\text{Fe}]$  for RGB stars from M08. *Right:*  $[\text{Na}/\text{Fe}]$  as a function of  $(B - I)$ .